

Article

Evaluation of Various Forms of Geothermal Energy Release in the Beijing Region, China

Zebin Luo ¹, Mingbo Yang ^{2,*}, Xiaocheng Zhou ^{3,*}, Guiping Liu ², Jinlong Liang ⁴, Zhe Liu ⁵, Peixue Hua ², Jingchen Ma ⁵, Leyin Hu ², Xiaoru Sun ², Bowen Cui ², Zhiguo Wang ² and Yuxuan Chen ²

¹ School of Emergency Management, Xihua University, Chengdu 610039, China; zebin_l@mail.xhu.edu.cn

² Beijing Earthquake Agency, Beijing 100080, China; liuguiping@bjseis.gov.cn (G.L.); huapeixue@bjseis.gov.cn (P.H.); huleyin@bjseis.gov.cn (L.H.); sunxr@bjseis.cn (X.S.); cuixie2001@bjseis.gov.cn (B.C.); wzg@bjseis.gov.cn (Z.W.); chenyx@bjseis.cn (Y.C.)

³ United Laboratory of High-Pressure Physics and Earthquake Science, Institute of Earthquake Forecasting, China Earthquake Administration CEA, Beijing 100036, China

⁴ College of Earth Science, Chengdu University of Technology, Chengdu 610059, China; richardljl04@aliyun.com

⁵ Beijing Institute of Geo-Engineering, Beijing 100048, China; liuzhedante@126.com (Z.L.); 13910656366@126.com (J.M.)

* Correspondence: yangmb2008@163.com (M.Y.); zhouxiaocheng188@163.com (X.Z.)

Abstract: The energy inside the Earth can not only be released outward through earthquakes and volcanoes but also can be used by humans in the form of geothermal energy. Is there a correlation between different forms of energy release? In this contribution, we perform detailed seismic and geothermal research in the Beijing area. The results show that the geothermal resources in Beijing belong to typical medium-low temperature geothermal resources of the sedimentary basin, and some areas are controlled by deep fault activities (e.g., Xiji geothermal well (No. 17)). The heat sources are upper mantle heat, radioactive heat in granite, and residual heat from magma cooling. The high overlap of earthquakes and geothermal field locations and the positive correlation between the injection water and earthquakes indicate that the exploitation and injection water will promote the release of the earth's energy. The energy releases are partitioned into multiple microearthquakes, avoiding damaging earthquakes ($M_L \geq 5$) due to excessive energy accumulation. Therefore, the exploitation of geothermal resources may be one way to reduce destructive earthquakes. Furthermore, the use of geothermal resources can also reduce the burning of fossil energy, which is of great significance in dealing with global warming.

Keywords: geothermal; earthquake forecasting; global warming; hot spring; Beijing; Zhangjiakou-Bohai fault



Citation: Luo, Z.; Yang, M.; Zhou, X.; Liu, G.; Liang, J.; Liu, Z.; Hua, P.; Ma, J.; Hu, L.; Sun, X.; et al. Evaluation of Various Forms of Geothermal Energy Release in the Beijing Region, China. *Water* **2024**, *16*, 622. <https://doi.org/10.3390/w16040622>

Academic Editor: Elias Dimitriou

Received: 22 December 2023

Revised: 9 February 2024

Accepted: 14 February 2024

Published: 19 February 2024



Copyright: © 2024 by the authors. Licensee MDPI, Basel, Switzerland. This article is an open access article distributed under the terms and conditions of the Creative Commons Attribution (CC BY) license (<https://creativecommons.org/licenses/by/4.0/>).

1. Introduction

The interior of the earth is filled with energy, which originates from the magma and the decay of radioactive materials. The energy can be released into the shallow surface or atmosphere in various ways. They can be fierce and destructive, like earthquakes and volcanoes, or relatively gentle, like hot springs. The difference is that earthquakes and volcanoes represent disasters, while hot springs are clean energy that can be used by humans. It is worth noting that they all originate from the release of energy inside the Earth. Is there a correlation between the different forms of energy release?

Unlike earthquakes and volcanoes, geothermal resources can be used by humans in a gentle way. Geothermal resources are considered one of the ways to combat global warming. The exploitation of geothermal resources has always been the focus of attention [1–11]. According to statistics, the geothermal energy reserves in the upper crust (3–10 km) are 1.3×10^{27} J. In the World Energy Association's "Energy and Sustainability Challenges" report published in 2000, geothermal energy ranked first among all renewable energy

sources [12]. However, induced earthquakes have been observed at various production stages of geothermal energy extraction, including initial injection of geothermal working fluid during stimulation, withdrawal of working fluid from geothermal reservoirs, reinjection of working fluid after heat extraction, and post-well closure [13]. Along with the disturbance of the crustal stress state, some exploitation projects have induced sizable earthquakes, even causing significant disasters and social problems [14–19]. For example, Soultz-Sous-Forêts in France [20], Basel in Switzerland [21], and Pohang in South Korea [22]. Therefore, exploring the mechanism of earthquakes induced by geothermal energy mining has been a hot topic in the world.

Efforts have long been made to mitigate or even eliminate induced earthquakes, whether from geothermal or oil and gas extraction. Induced seismicity is often perceived as an unsolicited and uncontrollable side effect of geothermal development [16,23–31]. But in fact, in most cases of induced seismicity, many events usually have magnitudes smaller than $M_L = 3$ and hence without economic consequences [15,32]. Seismicity triggered by fluid injection-induced earthquakes are still natural earthquakes, and their energy still comes from the Earth itself. Therefore, we put forward a conjecture: the total amount of Earth's energy is fixed, and earthquakes and geothermal are different forms of energy release. Is it possible to reduce the energy released by earthquakes by increasing the energy released by geothermal development?

To test the assumption, we choose the Beijing area for seismic and geothermal research. There are abundant geothermal resources in the Beijing area. Statistically, from 1971 to 2013, the total amount of geothermal resources exploitation quantity in Beijing is $2.87 \times 10^8 \text{ m}^3$, and the injection water is $3.02 \times 10^7 \text{ m}^3$ (Data from Beijing Geological Archive). In addition, there is a complete seismic network in the Beijing area, with detailed records of earthquakes ($M_L \geq 1$) since 1970. Therefore, Beijing is a natural laboratory for studying the relationship between seismic activity and geothermal energy.

2. The Study Area

The North China Craton (NCC) is one of the ancient cratons in the world [33]. It is bounded by the Central Asian orogenic belt in the north and the Qinling–Dabbe orogenic belt in the south. The basement rocks of the NCC consist of biotite-hornblende gneisses and Trondhjemite, Tonalite, Granodiorite (TTG) [34]. Overlying sedimentary layers with a thickness of several thousand meters, mainly carbonate rocks and clastic rocks. During the Yanshan tectonic period, the NCC experienced destruction and thinning, accompanied by a series of volcanic tectonic processes [35–39].

Beijing is located in the northern margin of NCC, high in the northwest and low in the southeast. Tectonic movement is active in the area [40]. The main faults include the Yanqing Fault, Dahucang Fault, Liangxiang Fault, and Zhangjiakou-Bohai Fault (Figure 1). It is a seismic activity zone in eastern China. In history, there has been the $M_L 7.8$ Tangshan earthquake (28 July 1978), the $M_L 7.4$ Bohai earthquake (18 July 1969), and the $M_L 8.0$ Shanhe-Pinggu earthquake (2 September 1679) [41].

Beijing area is enriched in geothermal resources [42]. At present, there are 10 geothermal fields: (1) Yanqing, (2) Xiaotangshan, (3) Houshayu, (4) Northwest district, (5) Tianzhu, (6) Lisui, (7) Southeast district, (8) Shuangqiao, (9) Liangxiang and (10) Fengheying geothermal field (Figure 1) [43]. The total geothermal resources are about $9.94 \times 10^{16} \text{ KJ}$, equivalent to $3.39 \times 10^9 \text{ t}$ of standard coal (Data from Beijing Geological Archive).

The terrestrial heat flow in Beijing ranges from 16.45 to 383.97 mW/m^2 , with an average value of 65.95 mW/m^2 . The geothermal gradient in the central area of the geothermal field is more than 3.0 $^\circ\text{C}/100 \text{ m}$. In some areas (Figure 1b, 5: Tianzhu and 6: Lishui), the geothermal gradient is more than 5 $^\circ\text{C}/100 \text{ m}$. The geothermal resources in Beijing belong to the medium and low-temperature hot water, and the temperature range is 25.0–118.5 $^\circ\text{C}$. The geothermal water is Na-HCO₃-SO₄ type water with a salinity between 500 and 700 mg/L, with a high content of F and SiO₂, containing a small amount of trace elements, which is used for medical treatment and health care.

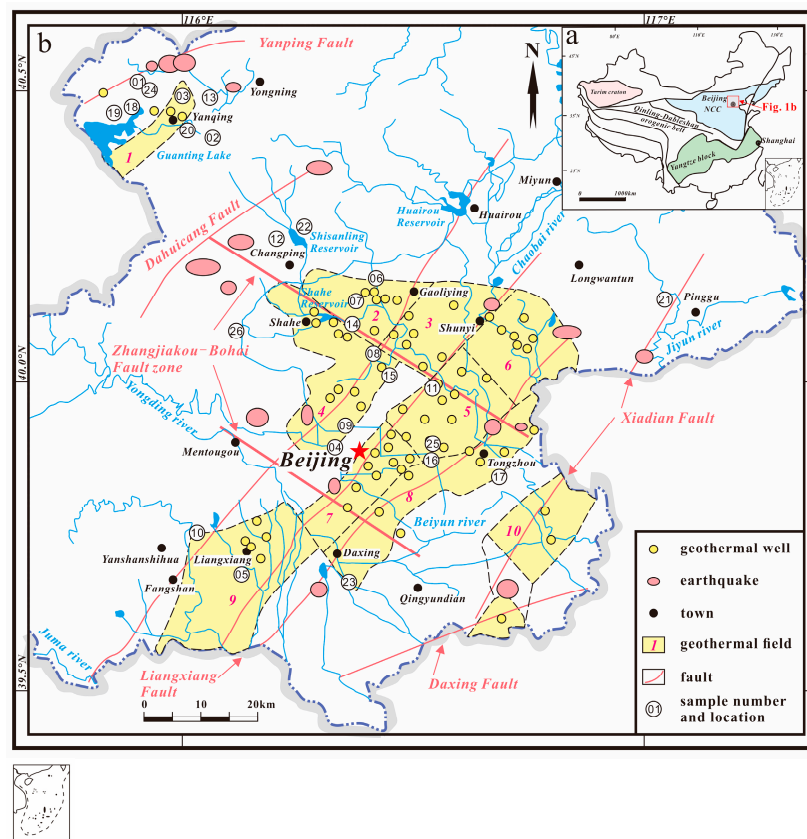


Figure 1. (a) A simple map of China. (b) Schematic map showing the distribution of geothermal fields and location of sampling points in the Beijing area, modified after Liu et al. [43]. 1: Yanqing, 2: Xiaotangshan, 3: Houshayu, 4: Northwest district, 5: Tianzhu, 6: Lishui, 7: Southeast district, 8: Shuangqiao, 9: Liangxiang and 10: Fengheying geothermal field. The size of the symbol of the earthquake label indicates the magnitude of the earthquake.

Beijing's climate is a warm, temperate, semi-humid, semi-arid monsoon climate, with an average annual temperature of 9 to 19 °C and annual precipitation of 600 mm. The seasonal distribution of precipitation is very uneven, with 80% of the annual precipitation concentrated in summer. The natural rivers of Beijing run through five major river systems from west to east: the Juma River, the Yongding River, the Beiyun River, the Chaobai River, and the Jiyun River. Most of them originated from the northwest mountain, meandered through the plain to the southeast, and finally merged into the Bohai Sea at the Haihe River.

3. Sampling and Analytical Methods

3.1. Geothermal Water Samples Collection and Analysis

Twenty-six samples of water were collected in Beijing, including hot springs and geothermal wells. All samples were analyzed for anions, cations, trace elements, hydrogen, and oxygen isotopes at the Beijing Institute of Geology of the Nuclear Industry. Detailed sample collection and testing methods can be found at Luo et al. [44]. In short, the waters were collected in a 50 mL clear polyethylene bottle, and the pH and temperature were recorded. Two water samples need to be collected at each geothermal water sampling site, one with ultrapure Nitric acid for cation analysis and the other for hydrogen and oxygen isotopes and anion analysis. Each sample is filtered with a 0.45 µm filter membrane before being tested. The cation and anion were analyzed by Dionex ICS-900 ion chromatograph (Thermo Fisher Scientific Inc., Bremen, Germany), and SiO₂ was analyzed by inductively coupled plasma emission spectrometer Optima-5300 DV (PerkinElmer Inc., Waltham, MA, USA). HCO₃⁻ and CO₃²⁻ was determined by acid-base titration with a ZDJ-100 potentiometric titrator. Trace elements were analyzed by Element XR ICP-MS. Multielement

standard solutions (IV-ICPMS 71A, IV-ICP-MS 71B and IV-ICP-MS 71D, iNORGANIC VENTURES) were used for quality control (the analytical error margin of major cations and trace elements were less than 10%). MAT 253 was used to analyze hydrogen and oxygen isotopes (reported as δD and $\delta^{18}O$ relative to Vienna Standard Mean Ocean Water (V-SMOW)).

3.2. Geothermal Gas Samples Collection and Analysis

Between April 2022 and April 2023, we collected geothermal gas samples five times at the No. 17 geothermal well. 500 mL glass bottles were used to collect gas by drainage gas collection method [44]. During transportation and storage, glass bottles are kept sealed to prevent contamination by air. The chemical composition of geothermal gas samples was measured using the Agilent Macro 490 portable gas chromatograph with a measurement accuracy of better than 5%. The concentration in hot spring gas samples was analyzed using the Noblesse noble gas isotope mass spectrometer by the Northwest Institute of Eco-Environmental Resources, Chinese Academy of Sciences.

4. Results and Discussion

4.1. Hydrochemistry of Geothermal Waters

The physical properties and chemical and isotopic compositions of geothermal waters are shown in Table S1. The temperature of water varies from 13 to 92 °C. In this study, we divided the samples into three groups according to the sampling sites (Figure 2). The first group of geothermal waters was distributed in the Beijing urban area, and the second group of geothermal waters was collected in the Yanqing basin. In particular, we also classified the geothermal water in group 3, which is similar to that in group 1 in terms of collection location but obviously different from that in group 1 in terms of hydrochemical characteristics. This will be discussed in detail below.

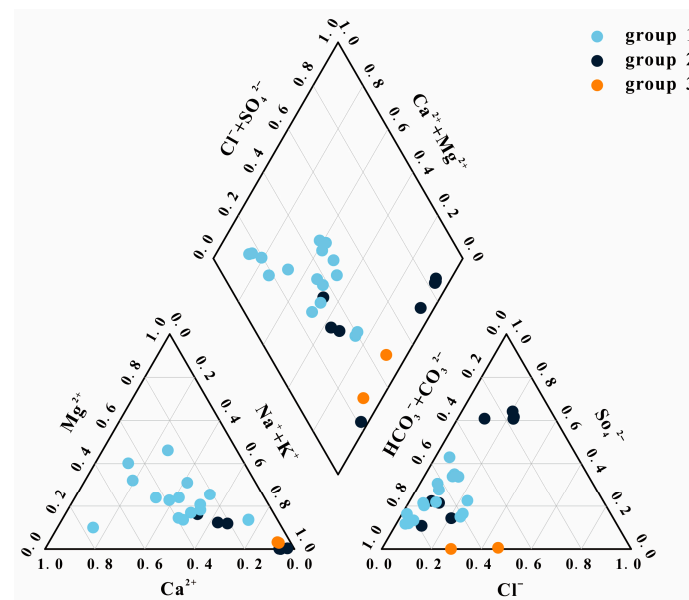


Figure 2. Piper diagram of geothermal waters in Beijing. These waters are Na-Ca-Mg-HCO₃, Na-SO₄, and Na-Cl types.

The $\delta^{18}O$ and δD of waters of Beijing are -16.2‰ to -9.6‰ and -92.4‰ to -69.2‰ respectively, which is close to the local meteoric water line (LMWL) of the Beijing $\delta D = 7.0181 \delta^{18}O + 3.5231$ ($R^2 = 0.86$, $n = 36$) (Figure 3) [45], suggesting they originated in meteoric. Group 2 is more enriched in light isotope composition than groups 1 and 3. The $\delta^{18}O$ value of a few waters went off the LMWL, indicating that the isotopic exchange of ^{18}O occurs during the water-rock reaction.

From Figure 2 and Table S1, the geothermal waters are Na-Ca·Mg-HCO₃ (group 1), Na-SO₄·HCO₃ (groups 2) and Na-Cl·HCO₃ (groups 3) types. Groups 2 have significantly higher concentrations of Na⁺ (84.50–151 mg/L) but lower Ca²⁺ (3.16–46.90 mg/L) and Mg²⁺ (0.04–14.8 mg/L) than group 1 (Na⁺ (5.41–135 mg/L), Ca²⁺ (19.20–57.50 mg/L) and Mg²⁺ (2.30–37.10 mg/L)), which may reflect the reaction between groundwater and silicate rocks (Figure 4). It is consistent with the fact that group 2 waters are located in the granite thermal reservoir of the Yanqing basin. Analogously, there were also differences between group 2 and group 3. The anions of group 2 are HCO₃⁻ (17.70–303 mg/L) and SO₄²⁻ (29.70–177 mg/L), while Group 3 contains more Cl⁻ (225–325 mg/L) and HCO₃⁻ (648–1022 mg/L). In the Paleogene period, the gypsum salt layer was widely distributed in the North China Plain [46]. The elevated concentration of SO₄²⁻ could be caused by the dissolution of sulfate minerals, such as anhydrite (CaSO₄) and mirabilite (Na₂SO₄). In addition, the high concentrations of Cl⁻ in geothermal water probably originated from brine or the mixing with a deep fluid [44,47,48]. However, in the Beijing area, the brine has almost no effect on Cl⁻. Because group 3 is well water located near the fault zone. The depth of 3588 m has exceeded the thickness of the sedimentary and reached the top of the magmatic batholith. Moreover, the Cl⁻ versus Na⁺ also indicates that the fluid is non-brined (Figure 5). Therefore, deep Cl⁻-rich magmatic fluids rise along faults and then mix with groundwater to form group 3 of geothermal waters with high Cl⁻ concentration.

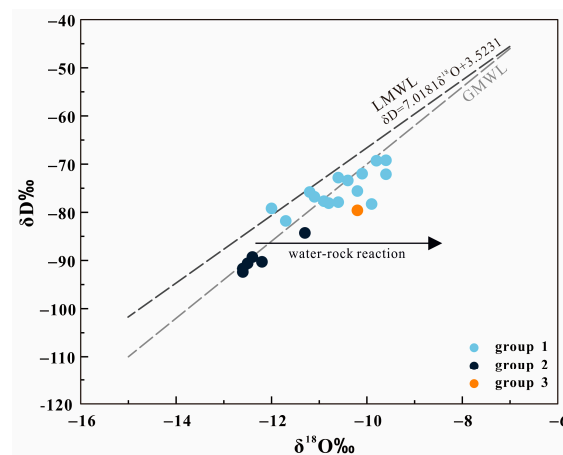


Figure 3. δD and δ¹⁸O (relative to V-SMOW) values for waters collected from the Beijing area. The GMWL is a global meteoric water line [49]. The LMWL is a local meteoric water line [45]. Arrows indicate enhanced water-rock reactions.

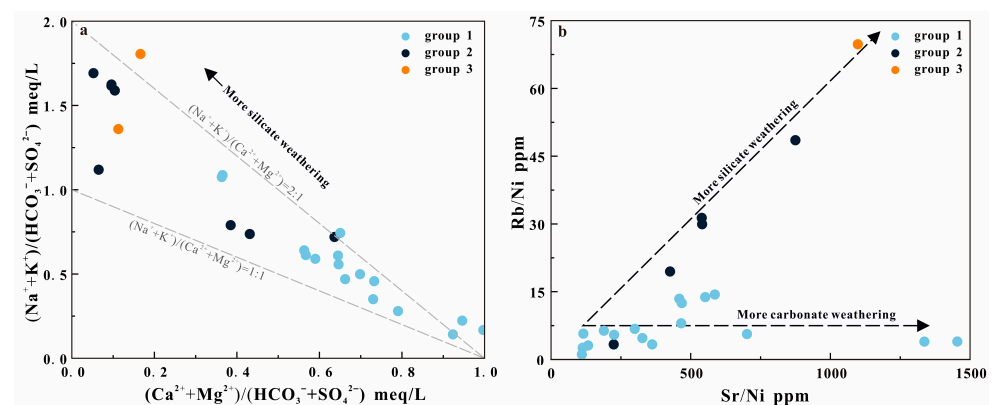


Figure 4. (Na⁺ + K⁺)/(HCO₃⁻ + SO₄²⁻) meq/L versus (Ca²⁺ + Mg²⁺)/(HCO₃⁻ + SO₄²⁻) meq/L (a) and Rb/Ni ppm versus Sr/Ni ppm (b) for geothermal waters of Beijing area. Group 1 is characterized by the reaction of carbonate rock with water, while groups 2 and 3 are characterized by the reaction of silicate rock with water.

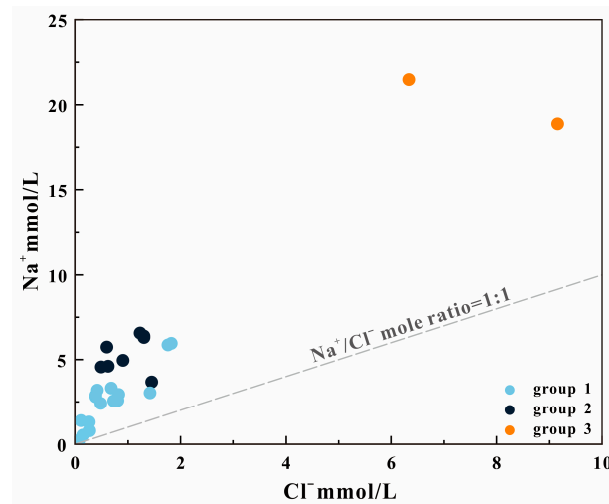


Figure 5. Na^+ versus Cl^- for Beijing area geothermal waters.

The sedimentary layer in the North China Plain is several thousand meters high, including carbonate and clastic rocks, which well explains the high Ca^{2+} and Mg^{2+} concentrations in group 1 (Table S1) [42,43,46]. Relatively, the sedimentary layer in the granite thermal reservoir of the Yanqing basin is thinner, and the Ca^{2+} and Mg^{2+} concentrations in group 2 are lower. It can be seen from Figure 4 that the weathering characteristics of the silicate rocks of group 2 geothermal waters are significantly greater than those of group 1. Rubidium (Rb) occurs preferentially in K-containing minerals, while Strontium (Sr) occurs preferentially in Ca-containing minerals, and Nickel (Ni) is an extremely compatible element. Using Ni as the regional background value to normalize Rb and Sr, the source of ions in geothermal water can be distinguished. As can be seen from Figure 4, groups 2 and 3 are characterized by the reaction of silicate rocks with water, while group 1 is characterized by the reaction of carbonate rocks with water.

Carbonate rocks, including limestone and dolomite, can be further distinguished by the variation of Ca^{2+} and Mg^{2+} content. The $\text{Mg}^{2+}/\text{Ca}^{2+}$ molar ratio of the geothermal water in the dolomite area is near one, while it is much lower than one in the limestone area [50]. Meanwhile, the $\text{Na}^+/\text{Ca}^{2+}$ molar ratio can distinguish the carbonate rock and silicate rock area. As shown in Figure 6, the geothermal water in Beijing mainly comes from dolomite and silicate rock, or a mixture of them, with almost no contribution from limestone.

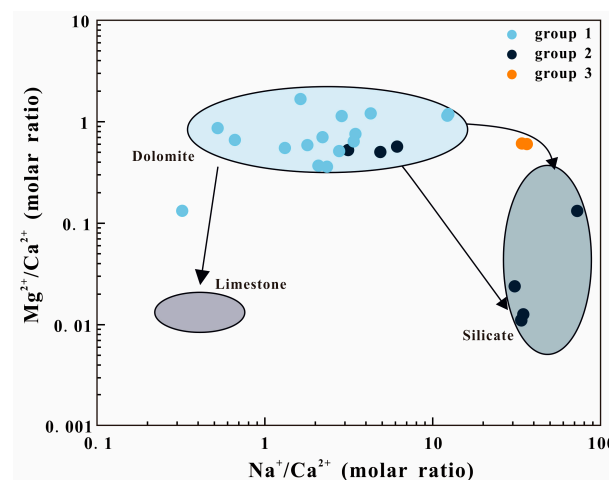


Figure 6. $\text{Mg}^{2+}/\text{Ca}^{2+}$ versus $\text{Na}^+/\text{Ca}^{2+}$ for geothermal waters of the Beijing area. The Dolomite, silicate, and limestone areas are from [50].

4.2. Characteristics of Heat Reservoir

The geothermal resources in Beijing belong to typical medium-low temperature geothermal resources of the sedimentary basin. The temperature varied from 25.0 to 118.5 °C, and the heat reservoirs are carbonate rocks [42]. The good thermal conductivity of carbonate rock results in a geothermal gradient in the study area (3–3.5 °C/100 m). All geothermal waters are plotted in the immature water field or partially equilibrated or mixed water (Figure S1). Therefore, pay attention to the applicability of the geothermometer when selecting the temperature scale. Previous studies have shown that the accuracy of the Na-Li geothermometer is higher than that of other thermometers in the carbonate rock region [44,51]. Therefore, the heat storage temperature of geothermal water in the study area was estimated by Na-Li geothermometer, and the results are shown in Table S2. Furthermore, quartz thermometers are also used as a reference [52]. The reservoir temperature and circulation depths of geothermal waters in the Beijing area calculated based on Na-Li and SiO₂ geothermometers are 65–240 °C and 1592–6597 m, respectively [44].

4.3. Origin of High He, H₂, and CH₄ Concentrations in Geothermal Gases

Yang et al. [40] observed that the No. 17 geothermal well has high concentrations of H₂ (330 ppm), He (5993 ppm), and CH₄ (volume ratio = 27.6%), and indicated that it may contain important information. Therefore, we have made a more in-depth study of No. 17 geothermal wells. Five samples were collected from the No. 17 geothermal well from April 2022 to April 2023. The chemical compositions of the geothermal gas samples are shown in Table S3 and Figure 7. N₂ and CH₄ account for more than 93% of No. 17 geothermal wells. He concentration (4243–6049 ppm) is significantly higher than other geothermal gases in the Beijing area (150–1851 ppm). What is the genesis of these high abnormal concentrations of these gas components? We will discuss this in detail below.

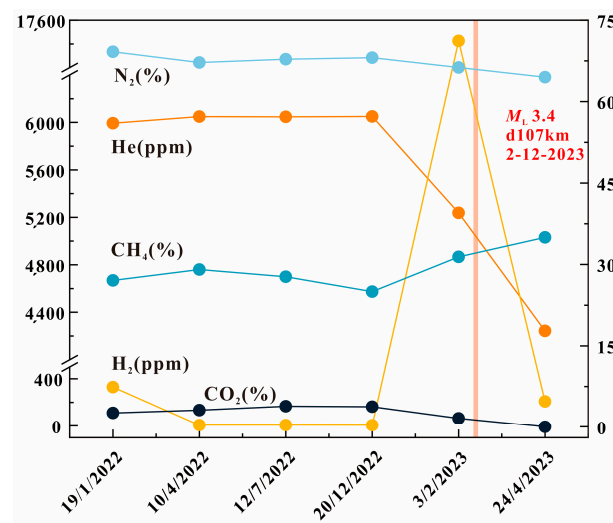


Figure 7. Characteristics of gas composition with time in Xiji (No. 17) geothermal well. Data of 19 January 2022 from Yang et al. [40].

4.3.1. He

As discussed earlier, the No. 17 geothermal water belongs to Group 3 and has a high Cl[−] concentration, which probably reflects the intensity of deep fluid activity. Helium is also a geochemical indicator of tectonic activity and earthquakes. Both tectonic activity and earthquakes release large amounts of He [44,53]. However, He suddenly descends into No. 17 geothermal water in response to a significant earthquake, which is different from the traditional understanding [54]. In fact, even if the He concentration was reduced from 6049 ppm to 4243 ppm, the He concentration at the No. 17 geothermal water was still much higher than that of other geothermal water in the Beijing area. The reason for the decrease

in He concentration before the earthquake may be that the faulting activity leads to the mixing of more air, diluting He in the geothermal gas. Therefore, the high He concentration of No. 17 geothermal gas should originate from deep fluid activity.

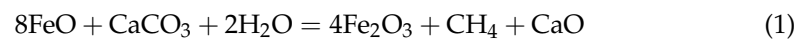
4.3.2. CH₄

Most of the world's methane is biotic CH₄, which is produced either by microbial processes or by thermogenic degradation of organic matter in sedimentary rocks [55,56]. However, there is another origin of CH₄, called abiogenic CH₄. It can be formed by chemical reactions that do not directly include organic matter [57–64]. Abiogenic CH₄ is extremely important in a wide range of scientific fields, including the origin of life, hydrocarbon synthesis, astrobiology, and planetary exploration [56].

During the Paleogene, oil shales were widely distributed in the Beijing area [46]. Does the high concentration of CH₄ in No. 17 geothermal gas originate from the thermogenic degradation of oil shales? Yes, but not entirely! Because well No. 17 had already cut through the sediment (3588 m, Table S1), and both Cl[−] and He indicate that No. 17 geothermal is polluted by deep fluid. In addition, deep tectono-magmatic activity, magma cooling, and gas-water-rock reactions can produce abiogenic CH₄ [56]. Hence, the gas of the No. 17 geothermal well should be coming from deeper and contain abiogenic CH₄. Although the δ¹³CH₄ of No. 17 is −36.4 [40], which shows the characteristics of biogenic CH₄ [56], it may be a mixed value. The mixture of abiogenic CH₄ from deep and biogenic CH₄ released by thermogenic degradation of oil shales formed geothermal gas No. 17.

What is the genesis of abiogenic CH₄ in geothermal gas No. 17? We propose that there are three ways:

- (1) Carbonate reacts with water in the presence of Fe (500–1500 °C) [56]:



- (2) CO₂ evolution to CH₄ during magma cooling (<500 °C) [56]:



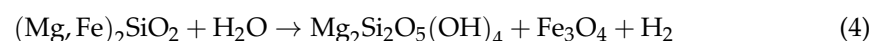
- (3) The Sabatier reaction (25–500 °C) [56]:



The sedimentary layer in the NCC is several thousand meters high, including carbonate and clastic rocks, which can provide sufficient CaCO₃ for (1). The (2) benefits from magmatic rocks produced by extensive Yanshanian magmatic activity [35,36,39]. The high concentration of H₂ and CO₂ in the geothermal gas of No. 17 provided the conditions for (3).

4.3.3. H₂

A large number of experiments and natural observations have shown that hydrogen can be produced by faulting movements [54,65–69]. The origin of H₂ is usually attributed to a chemical reaction between crushed silicate minerals and water (e.g., serpentinization produces molecular hydrogen (4)) [67,70], which enables H₂ to reflect the activity of the fault to a certain extent [40,54,71].



Olivine + fluid → serpentine + magnetite + hydrogen

Hydrogen content varies greatly in No. 17 geothermal gas. In particular, in the 3 February 2023 sample, a concentration of 17,426 ppm of H₂ was recorded, which probably reflects a precursory pulse of seismic activity (Figure 7). Sure enough, on 12 February 2023,

the ninth day after the signal was detected, 11 earthquakes were detected in the same place; the maximum magnitude was $M_L 3.4$, at a maximum depth of 14 km (Table S4).

Beijing area is located on the northern margin of NCC. During the Yanshan tectonic period, the NCC experienced destruction and thinning under the influence of Pacific subduction [33,35,36,39]. The resulting magmatic rocks and fault zones provide the material sources and ascending channels for hydrogen generation. The hydrogen production is controlled by the activity of the fault zone. Therefore, the H_2 concentration in No. 17 geothermal gas can be used for monitoring fault activity and earthquake warnings.

4.4. Geothermal Water Cycle Model and Genesis of Geothermal Field

As discussed above, the geothermal water in the Beijing area can be divided into three groups. Group 1 is located in the sedimentary area, dominated by $Na\cdot Ca\cdot Mg\cdot HCO_3$, and group 2 is located in the silicate rock area, dominated by $Na\cdot SO_4\cdot HCO_3$. In particular, although group 3 is located in the sedimentary area, the depth of 3588 m has exceeded the thickness of the sedimentary and reached the top of the magmatic rock batholith, so that group 3 has the characteristics of deep fluid with high Cl^- , He, H_2 and CH_4 . Combined with geochemical and isotopic composition, we propose that the geothermal water in the Beijing area originated from atmospheric precipitation. The precipitation flows into the ground along the fault and reacts with the surrounding rock while being heated. Eventually, they go up well along the fault to form hot springs (Figure 8). The geothermal resources in Beijing belong to typical medium-low temperature geothermal resources of the sedimentary basin, and some areas are controlled by deep fault activity (e.g., Xiji geothermal well (No. 17)). The heat sources are upper mantle heat, radioactive heat in granite and magmatic cooling residual heat. The heat reservoir is carbonate rock.

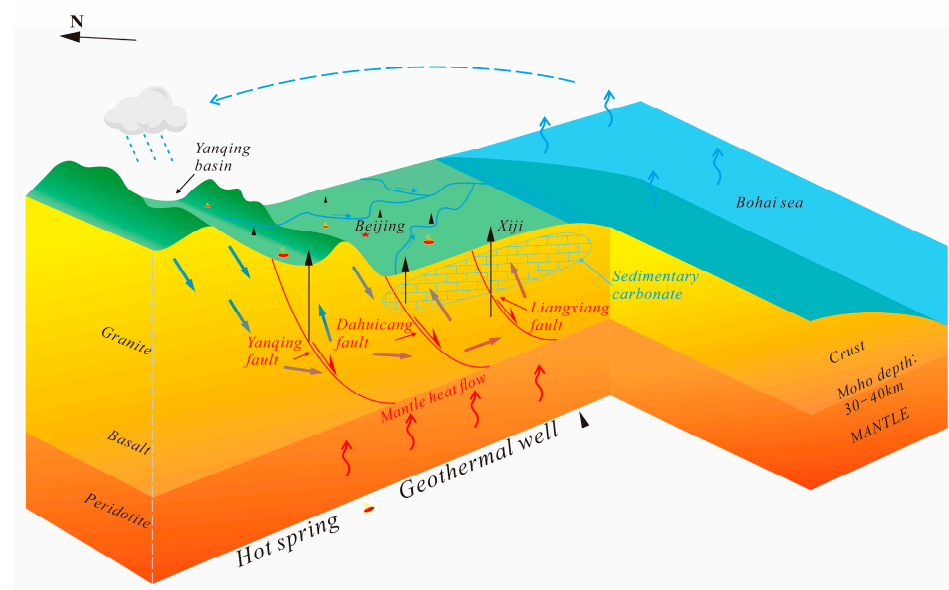


Figure 8. The water cycle model of the geothermal waters and gases in the Beijing area. The geothermal water in the Beijing area originated from atmospheric precipitation. The precipitation flows into the ground along the fault and reacts with the surrounding rock while being heated. Eventually, upwell along the fault to form hot springs.

4.5. The Promotion of Geothermal Resources to Promote the Earth's Energy Release

The way the earth releases energy can be geothermal energy or earthquakes. A large number of studies on oil and gas extraction, wastewater treatment, and geothermal exploitation have shown that fluids can promote seismic activity [14,15,17,23–32]. The geothermal development in the Beijing area includes the extraction and injection of water. So, what is the relationship between geothermal fluid activity and earthquakes?

the occurrence of destructive earthquakes. Therefore, we can reduce the occurrence of destructive earthquakes by rational use of geothermal resources.

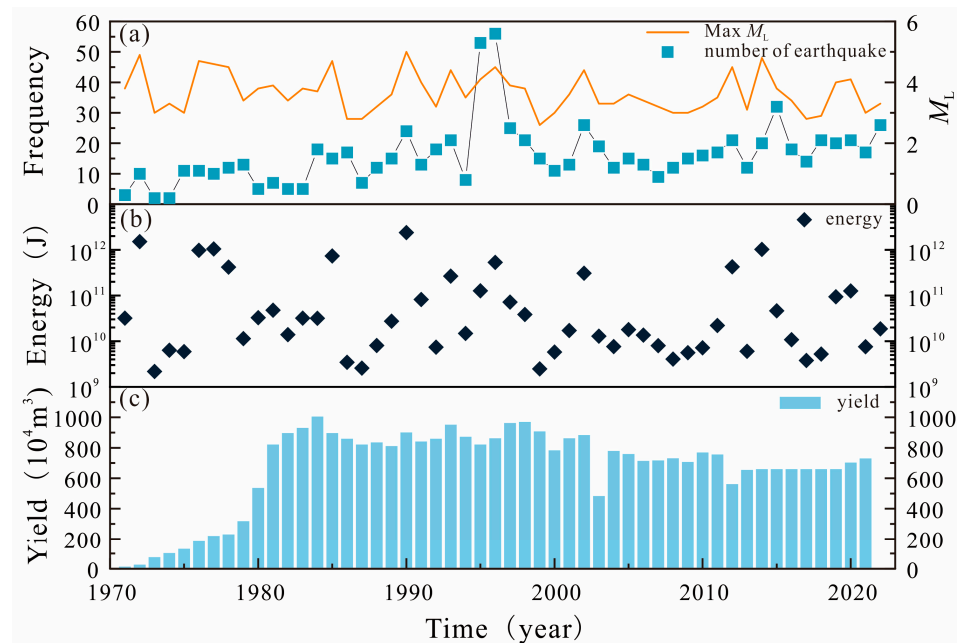


Figure 10. Temporal variations of earthquake frequency (time) (a), energy release (J) (b), and geothermal production (10^4 m^3) (c). The conversion formula of magnitude and energy: $\lg E = 4.8 + 1.5 M$, E is energy (J). M is magnitude ($M_L > 2$), earthquake data from the China Earthquake Administration. Geothermal production data from the Beijing Hydrogeological Engineering Team (2014–2019 are estimates).

5. Conclusions and Outlook

In this contribution, we perform a detailed elemental and isotopic analysis of geothermal waters and gases collected from the Beijing area. By integrating geochemical results of geothermal waters and gases, we propose that the geothermal resources in Beijing belong to typical medium-low temperature geothermal resources of the sedimentary basin, and some areas are controlled by deep fault activity (e.g., Xiji geothermal well (No. 17)).

The H_2 and CH_4 in the geothermal water/gas of the No. 17 geothermal well are sensitive to deep structural activities. By monitoring the elements and isotopes of geothermal well No. 17, the deep fluid activities can be reflected and thus forewarn earthquakes.

The extraction and injection of water will promote the release of Earth's energy. The energy is differentiated into multiple releases and avoids the excess accumulation of one-time energy, resulting in damaging earthquakes ($M_L \geq 5$). On the one hand, the exploitation of geothermal resources may be one way to reduce destructive earthquakes; on the other hand, the utilization of geothermal resources can reduce the consumption of fossil energy, which is of great significance for tackling global warming.

We propose that the exploitation of geothermal resources may be one of the means to reduce destructive earthquakes. However, given the complex thermal structure of the Earth's crust, the conversion mechanism between geothermal and seismic energy release is not known. Geothermal water links to earthquakes and to earthquake stress release are not established (no physical robust, statistical, or quantitative analyses). In addition, the study area is limited. Therefore, the contribution of this paper is that we provide a new research idea for earthquake and geothermal research, and more in-depth and systematic research is needed in the future.

Supplementary Materials: The following supporting information can be downloaded at: <https://www.mdpi.com/article/10.3390/w16040622/s1>, Table S1: Physical properties, hydrogeochemistry and isotopic compositions of geothermal waters from Beijing area; Figure S1: Na-K-Mg ternary diagram of geothermal waters in Beijing area; Table S2: Temperature results obtained with empirical chemical geothermometers (values in °C) and depths (m) of origin for Beijing area geothermal waters; Table S3: Geothermal gases chemistry compositions of Xiji geothermal well (No. 17) from Beijing area; Table S4: Earthquake records at 12 February 2023 in Beijing area; Figure S2: Relationship between volume of injection water (10^4 m^3) and number of earthquakes ($>M_L = 1$) in Beijing area.

Author Contributions: Conceptualization, Z.L. (Zebin Luo) and X.Z.; methodology, Z.L. (Zebin Luo); software, Z.L. (Zebin Luo); validation, X.Z. and J.L.; formal Analysis, X.Z.; investigation, M.Y., Z.L. (Zhe Liu), P.H., J.M., L.H., X.S., B.C., Z.W. and Y.C.; resources, M.Y.; data Curation, M.Y.; writing—Original Draft, Z.L. (Zebin Luo); writing—Review and Editing, Z.L. (Zebin Luo); supervision, X.Z.; project Administration, M.Y. and G.L.; funding acquisition, M.Y. All authors have read and agreed to the published version of the manuscript.

Funding: This work is supported by the surface technology project of Beijing earthquake agency (NO.BJMS-2024005) and Key Laboratory of Ionic Rare Earth Resources and Environment, Ministry of Natural Resources of the People’s Republic of China.

Data Availability Statement: Water and gas of hot springs data were measured by experimental instruments. Seismic records and geothermal resource data will be made available on request.

Acknowledgments: We would like to thank the Associate Editor and anonymous reviewers for their constructive comments, suggestions, and corrections. We also thank Lincheng Jiang and Tian Liang for the discussion.

Conflicts of Interest: The funders had no role in the design of the study, in the collection, analyses, or interpretation of data, in the writing of the manuscript, or in the decision to publish the results.

References

1. Alam, B.Y.C.S.S.S.; Itoi, R.; Taguchi, S.; Saibi, H.; Yamashiro, R. Hydrogeochemical and isotope characterization of geothermal waters from the Cidanau geothermal field, West Java, Indonesia. *Geothermics* **2019**, *78*, 62–69. [[CrossRef](#)]
2. Bahri, F.; Saibi, H.; Cherchali, M.-E.-H. Characterization, classification, and determination of drinkability of some Algerian thermal waters. *Arab. J. Geosci.* **2011**, *4*, 207–219. [[CrossRef](#)]
3. Elbarbary, S.; Zaher, M.A.; Saibi, H.; Fowler, A.-R.; Saibi, K. Geothermal renewable energy prospects of the African continent using GIS. *Geotherm. Energy* **2022**, *10*, 8. [[CrossRef](#)]
4. Saibi, H.; Batir, J.F.; Pocasangre, C. Hydrochemistry and geothermometry of thermal waters from UAE and their energetic potential assessment. *Geothermics* **2021**, *92*, 102061. [[CrossRef](#)]
5. Saibi, H.; Ehara, S. Temperature and chemical changes in the fluids of the Obama geothermal field (SW Japan) in response to field utilization. *Geothermics* **2010**, *39*, 228–241. [[CrossRef](#)]
6. Aboulela, H.; Amin, A.; Lashin, A.; El Rayes, A. Contribution of geothermal resources to the future of renewable energy in Egypt: A case study, Gulf of Suez-Egypt. *Renew. Energy* **2021**, *167*, 248–265. [[CrossRef](#)]
7. El-Rayes, A.E.; Arnous, M.O.; Aboulela, H.A. Hydrogeochemical and seismological exploration for geothermal resources in South Sinai, Egypt utilizing GIS and remote sensing. *Arab. J. Geosci.* **2015**, *8*, 5631–5647. [[CrossRef](#)]
8. Fan, Y.; Pang, Z.; Liao, D.; Tian, J.; Hao, Y.; Huang, T.; Li, Y. Hydrogeochemical Characteristics and Genesis of Geothermal Water from the Ganzi Geothermal Field, Eastern Tibetan Plateau. *Water* **2019**, *11*, 1631. [[CrossRef](#)]
9. Gu, X.M.; Zhang, Q.L.; Cui, Y.L.; Shao, J.L.; Xiao, Y.; Zhang, P.; Liu, J.X. Hydrogeochemistry and Genesis Analysis of Thermal and Mineral Springs in Arxan, Northeastern China. *Water* **2017**, *9*, 61. [[CrossRef](#)]
10. Deng, J.; Lin, W.; Xing, L.; Chen, L. The Estimation of Geothermal Reservoir Temperature Based on Integrated Multicomponent Geothermometry: A Case Study in the Jizhong Depression, North China Plain. *Water* **2022**, *14*, 2489. [[CrossRef](#)]
11. Yu, M.; Tian, X.; Zhang, H.; Li, J.; Wang, L.; Zhang, Z.; Lin, H.; Yang, X. Hydrogeochemical Characteristics of Geothermal Water in Ancient Deeply Buried Hills in the Northern Jizhong Depression, Bohai Bay Basin, China. *Water* **2023**, *15*, 3881. [[CrossRef](#)]
12. Yin, X.; Jiang, C.; Zhai, H.; Zhang, Y.; Jiang, C.; Lai, G.; Zhu, A.; Yin, F. Review of induced seismicity and disaster risk control in dry hot rock resource development worldwide. *Chin. J. Geophys. Chin. Ed.* **2021**, *64*, 3817–3836.
13. Okamoto, K.; Yi, L.; Asanuma, H.; Okabe, T.; Abe, Y.; Tsuzuki, M. Triggering processes of microseismic events associated with water injection in Okuaizu Geothermal Field, Japan. *Earth Planets Space* **2018**, *70*, 15. [[CrossRef](#)]
14. Brodsky, E.E.; Lajoie, L.J. Anthropogenic Seismicity Rates and Operational Parameters at the Salton Sea Geothermal Field. *Science* **2013**, *341*, 543–546. [[CrossRef](#)] [[PubMed](#)]
15. Gruenthal, G. Induced seismicity related to geothermal projects versus natural tectonic earthquakes and other types of induced seismic events in Central Europe. *Geothermics* **2014**, *52*, 22–35. [[CrossRef](#)]

16. Guglielmi, Y.; Cappa, F.; Avouac, J.P.; Henry, P.; Elsworth, D. Seismicity triggered by fluid injection-induced aseismic slip. *Science* **2015**, *348*, 1224–1226. [[CrossRef](#)]
17. Trutnevyte, E.; Wiemer, S. Tailor-made risk governance for induced seismicity of geothermal energy projects: An application to Switzerland. *Geothermics* **2017**, *65*, 295–312. [[CrossRef](#)]
18. Li, C.; Zhou, X.; Yan, Y.; Ouyang, S.; Liu, F. Hydrogeochemical Characteristics of Hot Springs and Their Short-Term Seismic Precursor Anomalies along the Xiaojiang Fault Zone, Southeast Tibet Plateau. *Water* **2021**, *13*, 2638. [[CrossRef](#)]
19. Wang, B.; Zhou, X.; Zhou, Y.; Yan, Y.; Li, Y.; Ouyang, S.; Liu, F.; Zhong, J. Hydrogeochemistry and Precursory Anomalies in Thermal Springs of Fujian (Southeastern China) Associated with Earthquakes in the Taiwan Strait. *Water* **2021**, *13*, 3523. [[CrossRef](#)]
20. Majer, E.L.; Baria, R.; Stark, M.; Oates, S.; Bommer, J.; Smith, B.; Asanuma, H. Induced seismicity associated with enhanced geothermal systems. *Geothermics* **2007**, *36*, 185–222. [[CrossRef](#)]
21. Haering, M.O.; Schanz, U.; Ladner, F.; Dyer, B.C. Characterisation of the Basel 1 enhanced geothermal system. *Geothermics* **2008**, *37*, 469–495. [[CrossRef](#)]
22. Kim, K.-H.; Ree, J.-H.; Kim, Y.; Kim, S.; Kang, S.Y.; Seo, W. Assessing whether the 2017 M_w 5.4 Pohang earthquake in South Korea was an induced event. *Science* **2018**, *360*, 1007–1009. [[CrossRef](#)]
23. Block, L.V.; Wood, C.K.; Yeck, W.L.; King, V.M. The 24 January 2013 M-L 4.4 Earthquake near Paradox, Colorado, and Its Relation to Deep Well Injection. *Seismol. Res. Lett.* **2014**, *85*, 609–624. [[CrossRef](#)]
24. Che, Y.; Yu, J. Influence and controlling of fluid in the crust on earthquake activity. *Recent Dev. World Seismol.* **2014**, *8*, 1–9, (In Chinese with English Abstract).
25. Ellsworth, W.L. Injection-Induced Earthquakes. *Science* **2013**, *341*, 142. [[CrossRef](#)] [[PubMed](#)]
26. Evans, D.M. Denver area earthquakes and the Rocky Mountain Arsenal disposal well. *Mt. Geol.* **1966**, *3*, 23–36.
27. Horton, S. Disposal of Hydrofracking Waste Fluid by Injection into Subsurface Aquifers Triggers Earthquake Swarm in Central Arkansas with Potential for Damaging Earthquake. *Seismol. Res. Lett.* **2012**, *83*, 250–260. [[CrossRef](#)]
28. Keranen, K.M.; Savage, H.M.; Abers, G.A.; Cochran, E.S. Potentially induced earthquakes in Oklahoma, USA: Links between wastewater injection and the 2011 M_w 5.7 earthquake sequence. *Geology* **2013**, *41*, 699–702. [[CrossRef](#)]
29. Keranen, K.M.; Weingarten, M.; Abers, G.A.; Bekins, B.A.; Ge, S. Sharp increase in central Oklahoma seismicity since 2008 induced by massive wastewater injection. *Science* **2014**, *345*, 448–451. [[CrossRef](#)] [[PubMed](#)]
30. Kim, W.Y. Induced seismicity associated with fluid injection into a deep well in Youngstown, Ohio. *J. Geophys. Res. Solid Earth* **2013**, *118*, 3506–3518. [[CrossRef](#)]
31. McGarr, A. Maximum magnitude earthquakes induced by fluid injection. *J. Geophys. Res. Solid Earth* **2014**, *119*, 1008–1019. [[CrossRef](#)]
32. Gaucher, E.; Schoenball, M.; Heidbach, O.; Zang, A.; Fokker, P.A.; Wees, J.D.V.; Kohl, T. Induced seismicity in geothermal reservoirs: A review of forecasting approaches. *Renew. Sustain. Energy Rev.* **2015**, *52*, 1473–1490. [[CrossRef](#)]
33. Gao, S.; Rudnick, R.L.; Yuan, H.L.; Liu, X.M.; Liu, Y.S.; Xu, W.L.; Ling, W.L.; Ayers, J.; Wang, X.C.; Wang, Q.H. Recycling lower continental crust in the North China craton. *Nature* **2004**, *432*, 892–897. [[CrossRef](#)] [[PubMed](#)]
34. Zhao, G.C.; Sun, M.; Wilde, S.A.; Li, S.Z. Late Archean to Paleoproterozoic evolution of the North China Craton: Key issues revisited. *Precambrian Res.* **2005**, *136*, 177–202. [[CrossRef](#)]
35. Ling, M.X.; Li, Y.; Ding, X.; Teng, F.Z.; Yang, X.Y.; Fan, W.M.; Xu, Y.G.; Sun, W.D. Destruction of the North China Craton Induced by Ridge Subductions. *J. Geol.* **2013**, *121*, 197–213. [[CrossRef](#)]
36. Wu, F.; Xu, Y.; Gao, S.; Zheng, J. Lithospheric thinning and destruction of the North China Craton. *Acta Petrol. Sin.* **2008**, *24*, 1145–1174, (In Chinese with English Abstract).
37. Zhu, R.; Chen, L.; Wu, F.; Liu, J. Timing, scale and mechanism of the destruction of the North China Craton. *Sci. China-Earth Sci.* **2011**, *54*, 789–797. [[CrossRef](#)]
38. Zhu, R.; Xu, Y.; Zhu, G.; Zhang, H.; Xia, Q.; Zheng, T. Destruction of the North China Craton. *Sci. China-Earth Sci.* **2012**, *55*, 1565–1587, (In Chinese with English Abstract). [[CrossRef](#)]
39. Zhu, R.X.; Xu, Y.G. The subduction of the west Pacific plate and the destruction of the North China Craton. *Sci. China-Earth Sci.* **2019**, *62*, 1340–1350. [[CrossRef](#)]
40. Yang, M.B.; Liu, G.P.; Liu, Z.; Ma, J.C.; Li, L.W.; Wang, Z.G.; Hua, P.X.; Xing, L.T.; Sun, X.R.; Han, K.Y.; et al. Geochemical characteristics of geothermal and hot spring gases in Beijing and Zhangjiakou Bohai fault zone. *Front. Earth Sci.* **2022**, *10*, 933066. [[CrossRef](#)]
41. Chen, F.; Guo, L.; Zhang, Z. Research on activity of Zhangjiakou-Bohai fault zone based on GPS observations. *Seismol. Geol.* **2020**, *42*, 95–108, (In Chinese with English Abstract).
42. Wang, G.; Zhang, W.; Lin, W.; Liu, F.; Zhu, X.; Liu, Y.; Li, J. Research on formation mode and development potential of geothermal resources in Beijing-Tianjin-Hebei region. *Geol. China* **2017**, *44*, 1074–1085, (In Chinese with English Abstract).
43. Liu, K.; Wang, S.; Sun, Y.; Cui, W.; Zhu, D. Characteristics and regionalization of geothermal resources in Beijing. *Geol. China* **2017**, *44*, 1128–1139, (In Chinese with English Abstract).
44. Luo, Z.; Zhou, X.; He, M.; Liang, J.; Li, J.; Dong, J.; Tian, J.; Yan, Y.; Li, Y.; Liu, F.; et al. Earthquakes evoked by lower crustal flow: Evidence from hot spring geochemistry in Lijiang-Xiaojinhe fault. *J. Hydrol.* **2023**, *619*, 129334. [[CrossRef](#)]
45. Zhai, Y.Z.; Wang, J.S.; Zhang, Y.; Teng, Y.G.; Zuo, R.; Huan, H. Hydrochemical and isotopic investigation of atmospheric precipitation in Beijing, China. *Sci. Total Environ.* **2013**, *456*, 202–211. [[CrossRef](#)] [[PubMed](#)]

46. Wang, X.X.; Zhou, X.R.; Li, S.H.; Zhang, N.D.; Ji, L.; Lu, H. Mechanism Study of Hydrocarbon Differential Distribution Controlled by the Activity of Growing Faults in Faulted Basins: Case Study of Paleogene in the Wang Guantun Area, Bohai Bay Basin, China. *Lithosphere* **2022**, *2021*, 7115985. [[CrossRef](#)]
47. Guo, Q.H. Hydrogeochemistry of high-temperature geothermal systems in China: A review. *Appl. Geochem.* **2012**, *27*, 1887–1898. [[CrossRef](#)]
48. Pan, S.; Kong, Y.; Wang, K.; Ren, Y.; Pang, Z.; Zhang, C.; Wen, D.; Zhang, L.; Feng, Q.; Zhu, G.; et al. Magmatic origin of geothermal fluids constrained by geochemical evidence: Implications for the heat source in the northeastern Tibetan Plateau. *J. Hydrol.* **2021**, *603*, 126985. [[CrossRef](#)]
49. Craig, H. Isotopic Variations in Meteoric Waters. *Science* **1961**, *133*, 1702–1703. [[CrossRef](#)]
50. Han, G.L.; Liu, C.Q. Water geochemistry controlled by carbonate dissolution: A study of the river waters draining karst-dominated terrain, Guizhou Province, China. *Chem. Geol.* **2004**, *204*, 1–21. [[CrossRef](#)]
51. Fouillac, C.; Michard, G. Sodium/lithium ratio in water applied to geothermometry of geothermal reservoirs. *Geothermics* **1981**, *10*, 55–70. [[CrossRef](#)]
52. Fournier, R.O. Chemical geothermometers and mixing models for geothermal systems. *Geothermics* **1977**, *5*, 41–50. [[CrossRef](#)]
53. Zhou, X.; Wang, W.; Chen, Z.; Yi, L.; Liu, L.; Xie, C.; Cui, Y.; Du, J.; Cheng, J.; Yang, L. Hot Spring Gas Geochemistry in Western Sichuan Province, China after the Wenchuan Ms 8.0 Earthquake. *Terr. Atmos. Ocean. Sci.* **2015**, *26*, 361. [[CrossRef](#)]
54. Zhou, X.C.; Yan, Y.C.; Fang, W.Y.; Wang, W.L.; Shi, H.Y.; Li, P.F. Short-Term Seismic Precursor Anomalies of Hydrogen Concentration in Luojishan Hot Spring Bubbling Gas, Eastern Tibetan Plateau. *Front. Earth Sci.* **2021**, *8*, 586279. [[CrossRef](#)]
55. Beaudry, P.; Stefansson, A.; Fiebig, J.; Rhim, J.H.; Ono, S. High temperature generation and equilibration of methane in terrestrial geothermal systems: Evidence from clumped isotopologues. *Geochim. Cosmochim. Acta* **2021**, *309*, 209–234. [[CrossRef](#)]
56. Etiope, G.; Lollar, B.S. Abiotic methane on earth. *Rev. Geophys.* **2013**, *51*, 276–299. [[CrossRef](#)]
57. Etiope, G.; Schoell, M. Abiotic Gas: Atypical, But Not Rare. *Elements* **2014**, *10*, 291–296. [[CrossRef](#)]
58. Etiope, G.; Schoell, M.; Hosgormez, H. Abiotic methane flux from the Chimaera seep and Tekirova ophiolites (Turkey): Understanding gas exhalation from low temperature serpentinization and implications for Mars. *Earth Planet. Sci. Lett.* **2011**, *310*, 96–104. [[CrossRef](#)]
59. Etiope, G.; Tsikouras, B.; Kordella, S.; Ifandi, E.; Christodoulou, D.; Papatheodorou, G. Methane flux and origin in the Othrys ophiolite hyperalkaline springs, Greece. *Chem. Geol.* **2013**, *347*, 161–174. [[CrossRef](#)]
60. Klein, F.; Grozeva, N.G.; Seewald, J.S. Abiotic methane synthesis and serpentinization in olivine-hosted fluid inclusions. *Proc. Natl. Acad. Sci. USA* **2019**, *116*, 17666–17672. [[CrossRef](#)]
61. McDermott, J.M.; Seewald, J.S.; German, C.R.; Sylva, S.P. Pathways for abiotic organic synthesis at submarine hydrothermal fields. *Proc. Natl. Acad. Sci. USA* **2015**, *112*, 7668–7672. [[CrossRef](#)] [[PubMed](#)]
62. Proskurowski, G.; Lilley, M.D.; Seewald, J.S.; Fruh-Green, G.L.; Olson, E.J.; Lupton, J.E.; Sylva, S.P.; Kelley, D.S. Abiogenic hydrocarbon production at Lost City hydrothermal field. *Science* **2008**, *319*, 604–607. [[CrossRef](#)] [[PubMed](#)]
63. Reeves, E.P.; Fiebig, J. Abiotic Synthesis of Methane and Organic-Compounds in Earth’s Lithosphere. *Elements* **2020**, *16*, 25–31. [[CrossRef](#)]
64. Sciarra, A.; Saroni, A.; Etiope, G.; Coltorti, M.; Mazzarini, F.; Lott, C.; Grassa, F.; Italiano, F. Shallow submarine seep of abiotic methane from serpentinized peridotite off the Island of Elba, Italy. *Appl. Geochem.* **2019**, *100*, 1–7. [[CrossRef](#)]
65. Di Martino, R.M.R.; Camarda, M.; Gurrieri, S.; Valenza, M. Continuous monitoring of hydrogen and carbon dioxide at Mt Etna. *Chem. Geol.* **2013**, *357*, 41–51. [[CrossRef](#)]
66. Hirose, T.; Kawagucci, S.; Suzuki, K. Mechanoradical H₂ generation during simulated faulting: Implications for an earthquake-driven subsurface biosphere. *Geophys. Res. Lett.* **2011**, *38*, L17303. [[CrossRef](#)]
67. Kameda, J.; Saruwatari, K.; Tanaka, H. H₂ generation in wet grinding of granite and single-crystal powders and implications for H₂ concentration on active faults. *Geophys. Res. Lett.* **2003**, *30*, 2063. [[CrossRef](#)]
68. Wakita, H.; Nakamura, Y.; Kita, I.; Fujii, N.; Notsu, K. Hydrogen release: New indicator of fault activity. *Science* **1980**, *210*, 188–190. [[CrossRef](#)]
69. Zhou, X.; Du, J.; Chen, Z.; Cheng, J.; Tang, Y.; Yang, L.; Xie, C.; Cui, Y.; Liu, L.; Li, Y.; et al. Geochemistry of soil gas in the seismic fault zone produced by the Wenchuan Ms 8.0 earthquake, southwestern China. *Geochem. Trans.* **2010**, *11*, 5. [[CrossRef](#)]
70. Huang, R.; Shang, X.; Zhao, Y.; Sun, W.; Liu, X. Effect of Fluid Salinity on Reaction Rate and Molecular Hydrogen (H₂) Formation during Peridotite Serpentinization at 300 °C. *J. Geophys. Res. Solid Earth* **2023**, *128*, e2022JB025218. [[CrossRef](#)]
71. Skelton, A.; Andren, M.; Kristmannsdottir, H.; Stockmann, G.; Morth, C.-M.; Sveinbjornsdottir, A.; Jonsson, S.; Sturkell, E.; Gudorunardottir, H.R.; Hjartarson, H.; et al. Changes in groundwater chemistry before two consecutive earthquakes in Iceland. *Nat. Geosci.* **2014**, *7*, 752–756. [[CrossRef](#)]

Disclaimer/Publisher’s Note: The statements, opinions and data contained in all publications are solely those of the individual author(s) and contributor(s) and not of MDPI and/or the editor(s). MDPI and/or the editor(s) disclaim responsibility for any injury to people or property resulting from any ideas, methods, instructions or products referred to in the content.